

ESTIMATES OF LOCAL VORTICITY IN MESOSCALE SYSTEMS

T.C. Granata, T.D. Dickey
 Ocean Physics Group
 University of Southern California
 Los Angeles CA, 90089-0740
 USA

M. Estrada and A. Castellon
 Institut de Ciències del Mar (CSIC)
 P. Nacional s/n
 08039 Barcelona
 Spain

Abstract

Changes in vertical shear, horizontal kinetic energy, and indices of vorticity (the depths of isothermal and isopycnal surfaces) were used to identify mesoscale variability in oceanic systems. Time series data from an area of high eddy activity (the re-circulation region of the Gulf Stream) and synoptic hydrographic data from a broad, meandering front (in the Catalan Sea) illustrate how indices of mesoscale variability can be used to estimate local changes in vorticity either from changes in height between isothermal/isopycnal surfaces, h , or from both h and direct current measurements.

For the Sargasso Sea time series, satellite images of sea surface height and estimates of local vorticity qualitatively agreed with indices of relative vorticity. Potential vorticity across the Catalan front also showed the same trend as the vorticity index.

1. Introduction

Recent advances in the development of towed conductivity-temperature-depth (CTD) instrumentation (Woods, 1988, Strass and Woods, 1988, Washburn et al., 1993), moored current meters (Weller, 1990, Dickey, 1991), and acoustic Doppler current profilers (Joyce et al., 1982; Reigier, 1982; Castellon, 1990) make it feasible to sample mesoscale density and current structures associated with eddies and fronts in the open ocean. These mesoscale features have temporal and spatial scales on the order of days and 100 Km, respectively.

Of particular importance in the dynamics of fronts and eddies is the vorticity of the flow field. Fischer et al. (1989) have proposed that, on mesoscales, vorticity can be determined from the relationship of conservation of vorticity a vortex tube:

$$q = \frac{\Delta\rho}{\rho \frac{\zeta+f}{H}}$$

and for a constant q ,

$$/h_o = \frac{\zeta}{f} \quad (1b)$$

where q is the potential vorticity between streamlines, ζ is the relative vorticity, f is the planetary vorticity, h is the distance between two isopycnals (assumed to approximate streamlines), $\Delta\rho$ is the density difference between the isopycnals, ρ_o is the mean density between the isopycnals, h_o height between the isopycnals when $\zeta = f$ (when the flow is in Sverdrup balance), and $H = h + h_o$. On an f -plane, increases in the relative vorticity (cyclonic changes) would increase the height between isopycnals while decreases in relative vorticity (anticyclonic changes) would force isopycnals closer together.

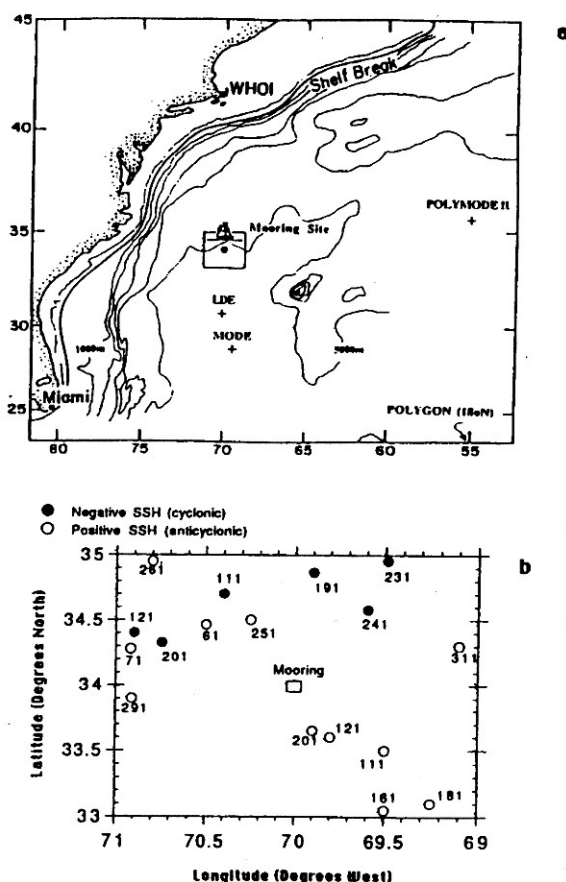


Figure 1. a. A map of the Northwestern Atlantic Ocean showing locations of various research sites. The Biowatt mooring, where time series data were collected, was located at 34°N, 70°W. (Redrawn from Dickey et al., 1991). The inset shows the location of sea surface height (SSH) data. b. Locations and times (in Julian days) of the centroid of SSH anomalies around the Biowatt mooring. Open circles indicate SSH elevations associated with warm water outbreaks of the Gulf Stream and anticyclonic circulation. Black circles represent SSH depressions resulting from advection of cold water and

This paper examines if simple indices of vorticity, based on the above relationships between h and z , are valid for the detection of changes in q from two distinctly different oceanic regions based on either moored time series or synoptically sampled hydrographic grid data. In the first region, the Sargasso Sea, a time series was collected at a station located at 34°N, 70°W. This site is on the Hatteras abyssal plain, 300 Km south of the main axis of the Gulf Stream and 120 Km southeast of the shelf slope. The region is a corridor for meandering cyclonic and anticyclonic eddies which form on the eastern and southern wall of the Gulf Stream (Richardson, 1983). The physical oceanography of this region has been well studied during such programs as POLYMODE (Hau et al., 1986) and MODE (MODE Group, 1978), and, at this particular station, during the LOTUS (Briscoe et al., 1984) and BIOWATT (Dickey et al., 1986) experiments (Figure 1a).

The second region was the Catalan Sea, in the northwestern basin of the Mediterranean Sea, where a hydrographic grid was sampled across a front between the Balearic Islands and the coast of the Iberian Peninsula (Figure 2a). This region is the location of a permanent central dome of dense water with less dense water along the shelf margins (Font et al., 1988; Estrada and Margalef, 1988). The Catalan current lies to the west of the dome and flows to the southwest along the continental slope (Salat and Font, 1987; Castellon et al., 1990). The Balearic current lies to east of the dome and flows to the northeast along the shelf margin of the Balearic Islands. The density structure and the counter flow of the two currents are consistent with maintenance of cyclonic motions in the central region of the dome (Font et al., 1988).

2. Methods

Moored measurements were taken during the BIOWATT II Experiment, 1987, in the Sargasso Sea (34°N, 70°W; Figure 1a) using the multi-variable moored system, MVMS (Dickey et al., 1991). Eight MVMS's were deployed at nominal depths of 10, 20, 40, 60, 80, 100, 120, and 160 m during three deployments over spring, summer, and fall of 1987. Among the physical parameters sampled were temperature and horizontal currents, u and v . Conductivity sensors did not function correctly and, therefore, no salinity data were available (for a full account of others parameters sampled see Dickey et al., 1991). MVMS data was averaged and recorded every 4 min for 260 days. After data were calibrated and corrected for spurious points, missing data (a maximum of 5 days between deployment periods) were filled by first calculating means of 10 day windows on each side of the gaps, fitting a spline curve to the means, and then superimposing the variance in the windows onto the curve. The resulting time series was smoothed with a 76 hour Gaussian filter, to remove inertial and diurnal signals, then averaged to 24 hour points using a box car method.

Maps of sea surface height (SSH) variability, calculated from satellite data (GEOSAT altimeter data), averaged over 10 days and 0.25° windows (Chai et al., 1992; Dickey et al., 1993), were used to determine the position of SSH anomalies (eddies) relative to the position of the Biowatt mooring. This was accomplished by measuring the distance between the mooring and the centroid of each anomaly for 25 images corresponding to 250 days during the Biowatt time series (Figure 1b).

Data from the Catalan Sea were collected during the Fronts 91 experiment in April, 1991 (Figure 2a). Temperature, salinity, and pressure were measured at seventy hydrographic stations using a Sea-Bird model 25 CTD. Data were recorded at 1 m intervals from 10m to a maximum depth of 400 m (150 m in the coastal zone). Stations were approximately 6.6 km apart and the entire 72 x 72 Km grid was sampled in 2.5 days (see Figure 2b). An acoustic Doppler current profiler (ADCP; RDI Inc.) mounted in the hull of the research vessel B/O Garcia del Cid provided $u(z)$ and $v(z)$ velocity components as the ship traversed each transect. Velocity data were collected every 1.28 seconds and averaged to 5 minute points for 50, 8 m depth bins. Velocities were referenced to ship position, measured using a Global Positioning System (GPS), and are accurate to within $\pm 2\text{cms}^{-1}$. Because of malfunctions of the ADCP during transects T1-T4 velocities across the front are not available for the southern portion of the grid. However, ADCP data were collected across the entire front

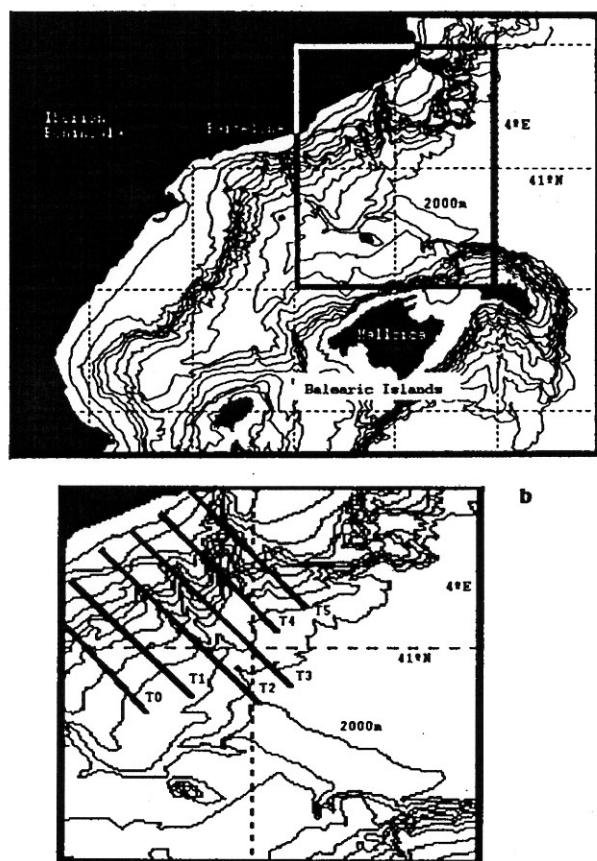


Figure 2. a. A map of the Catalan Sea with an inset showing the locations of hydrographic stations during the Frons 91 study. b. An enlargement of the inset showing the ship tract across hydrographic stations. Transects were approximately 14 Km apart and hydrographic stations along the transect 6.6 Km apart.

was for transect T5. Relative vorticity across transect T5 was calculated as $\zeta = \frac{\partial v}{\partial x} - \frac{\partial u}{\partial y}$, where x was normal to the coast and y parallel to the coast.

For both data sets, the absolute value of the vertical current shear was calculated as

$$\left| \frac{\partial u}{\partial z} \right| + \left| \frac{\partial v}{\partial z} \right| \quad (2)$$

where z is depth. Horizontal kinetic energy (HKE), at a given depth, was calculated as

$$\frac{u^2 + v^2}{2} \quad (3)$$

Since salinity time series, and hence isopycnal data, were not available for the Sargasso Sea time series, isotherms were used to calculate vorticity indices. The assumption made in this calculation was that vertical density distributions in the upper 200 meters of this region (but below the mixed layer) were more dependent on temperature than salinity changes. We justified this assumption

by noting the maximum temperature difference through a cross section of an eddy (for example from Sargasso water to the center of an eddy) accounts for a 3.5 kg m^{-3} density change while maximum salinity differences account for less than a 1.0 kg m^{-3} change. Thus, temperature can be used as a first order estimation of vertical motions of isopycnals. Depths of isotherms were calculated by interpolating a cubic spline curve fit to temperature profiles. Isotherms which spanned the majority of the time series ($20\text{--}21.5^\circ\text{C}$) were used to calculate vorticity indices. Two indices of vorticity were calculated based on the relationship between conservation of vorticity and the height separating two isopycnals. The first mesoscale index,

$$\frac{h}{h_o} \quad (4)$$

was used to estimate the change in height between two isotherms over the duration of the time series. Equation 4 differs from equations 1a, b in that: 1) h is the height between isotherms and not isopycnals; and 2) h_o was calculated as a linear curve fit to the h time series to account for seasonal changes in isotherm thickness (see Figure 3b). The removal of the seasonal trend was a two part process. First, a fourth order polynomial was fit to the time series ($r=0.78$) and each point differenced. The resulting time series had two periods with different slopes corresponding to the change in the net heat flux on day 225 (Dickey et al., 1993). One linear equation was fit to each period (before and after day 225) and the points differenced to give Figure 3c. The time derivative of the detrended data was used to define periods of upward motion (designated positive values or upwelled, U), downward motion (negative values or downwelled, D) and transition periods of pre-upwelled and pre-downwelled (PU and PD respectively) states.

The second index of vorticity was calculated only for time series data,

$$\frac{\langle T \rangle}{z_o} \left(\frac{dT}{dz} \right)^{-1} \quad (5)$$

where $\frac{dT}{dz}$ is the temperature gradient between 80 and 100 m (these depths were chosen to coincide with the depths of the isotherms used in equation 4), z_o is the average depth, and $\langle T \rangle$ is the average (i.e. seasonal) trend in isotherms which was estimated using a third order polynomial fit to the normalized temperature gradient. This index was greater than 1 when the number of isotherms between 80 and 100 m were less than the seasonal mean.

For the hydrographic grid, only one index of vorticity was calculated, equation 1b, and only for isopycnal data (σ_t). This was because indices derived from isotherms were less accurate in depicting vertical motions as a result of the dependence of density not only on temperature but also on salinity along the front (nominal changes of 2.0 psu). Depths of isopycnals were interpolated using a least squares regression on triangulated points. The index of relative vorticity, $\frac{h}{h_o}$, was calculated as the height between the 28.8 and 28.7 kg m^{-3} isopycnals, relative to the average height of isopycnals aligned parallel to the flow field and the coast.

3. Results

Time series, Sargasso Sea data.

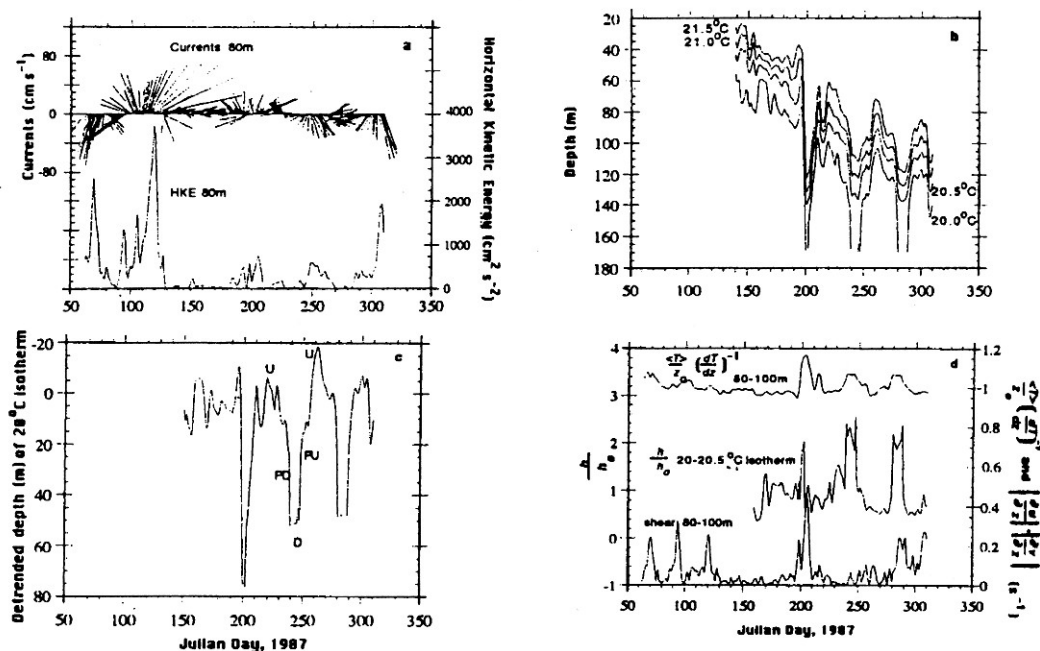


Figure 3. a. Time series of moved currents and horizontal kinetic energy (HKE) at 80 m. b. Time series of isotherms. c. The 20°C isotherm differenced from the seasonal trend, with examples of negative upwelled periods (U), positive downwelled periods (D), and transitional periods of pre-upwelled (PU) and pre-downwelled (PD). d. Time series of the absolute values the vertical current shear, $|\frac{\partial u}{\partial z}| + |\frac{\partial v}{\partial z}|$, and indices of vorticity, $\frac{h}{h_0}$ and $\frac{\partial T}{\partial z} \left(\frac{dT}{dz} \right)^{-1}$. Changes in cyclonic relative vorticity is depicted as indices greater than 1 and in anticyclonic relative vorticity by values less than 1.

Figure 1b shows the position and time of positive and negative SSH anomalies in an area 222 Km², roughly 2 eddy diameters square. Positive SSH anomalies (maximum of 30 cm) were associated with warm water outbreaks of the Gulf Stream and anticyclonic (clockwise) motion while negative anomalies (minimum of -30 cm) indicated cold water features associated with cyclonic motions (counter clockwise) (Dickey et al., 1993). Currents and HKE at 80 m indicated advective events that corresponded to SSH anomalies on days 60-70, 111-121, 161, 181, 191, 201, 250-260, and 290-310 (Figure 3a).

Vertical motions of isotherms also showed variability associated with mesoscale features (Figure 3a,b). The upward and downward motions of the 20°C isotherm were evident when the seasonal heating trend was removed (Figure 3c). The 20-20.5°C isotherms, which were below the nominal depth of the mixed layer (40 m), appeared to be good indicators of vorticity.

Time series of vorticity indices also showed variability on the same scales as HKE and isotherms (Figure 3d). High indices of vorticity, on days 195-205 and 231-241, were coincident with cyclonic motion about SSH depressions. No SSH data was available for day 280 when the indices were again high, however, a cyclonic eddy was present to the northeast and an anticyclonic eddy to the southeast of the mooring on day 271 (Dickey et al., 1993). Given that, on the average, eddies in this region meander to the southwest (Richardson, 1983), it is likely the cyclonic eddy on day 271 may have moved into the mooring site by day 280 accounting for the advection of isotherms and increases in HKE and vorticity indices. Vorticity indices were lowest on days 161, 202-210, 261, and

300-311 coincident with anticyclonic motions about SSH elevations.

Since vertical shear is proportional to horizontal advection of temperature, (Gill, 1982),

$$\left| \frac{\partial u}{\partial z} \right| + \left| \frac{\partial v}{\partial z} \right| \propto \frac{1}{\langle T \rangle} \left(\frac{\partial T}{\partial x} - \frac{\partial T}{\partial y} \right) \quad (6)$$

strong thermal advection, associated with eddies and fronts, should be also be related to indices of vorticity. A plot of absolute vertical current shear between 80-100 m (Figure 3d) revealed high shear during periods of high HKE and vorticity. Decorrelation time scales, based on the first zero crossing of the autocorrelations, were 15-16 days for shear and HKE time series and 8-10 days for both indices of vorticity.

Table 1. Summary of analysis of variance for time series with the means (of sample size n) for each parameter and category.

Parameters	upwelled $n=32$	downwelled $n=60$	pre-upwelled $n=38$	pre-downwelled $n=31$	F statistic
$\frac{h}{h_0}$	0.44*	1.18*	0.87	0.83	9.40
$\frac{\partial}{\partial z} \left(\frac{dT}{dz} \right)^{-1}$	0.97*	1.02	1.02	1.01	7.02
HKE	160	194	378**	235	3.46
$\left \frac{\partial u}{\partial z} \right + \left \frac{\partial v}{\partial z} \right $	0.04	0.06	0.13*	0.06	8.64

* $p = .0001$

** $p = .018$

Results of an analysis of variance (ANOVA using 5 day means) for the indices of vorticity, HKE, and shear are shown in Table 1 for each category of temperature change: U, upwelled, D, downwelled, PU, pre-upwelled, and DU, pre-downwelled. Both indices of vorticity, $\frac{h}{h_0}$ and $\frac{\partial}{\partial z} \left(\frac{dT}{dz} \right)^{-1}$, showed highly significant anticyclonic motions during upwelling periods, however, only $\frac{h}{h_0}$ correlated with cyclonic motion associated with downwelling periods. Higher values of shear and HKE were significantly correlated with pre-upwelling events.

Hydrographic surveys, Catalan Sea data.

Figure 4a shows ADCP currents measured at 22 m for transect T5. Currents along the coast were generally directed to the southwest with maximum velocities of 18 cm s^{-1} . Currents farthest from the coast, between 70-80 Km, were directed to the southeast with maximum velocities of 24 cm s^{-1} . Between 40 and 70 Km from the coast, near surface currents rotated counterclockwise, indicating a positive vorticity.

The vertical distribution of ρ along transect T5, from Barcelona (Spain) to the Balearic Islands, showed a dome of isopycnals between 40-70 Km (Figure 4b). Isopycnal domes were present along all transects but the position of the dome along the transects, varied from 25 to 65 Km as the front meandered in the along coast direction. Generally, surface waters ($\leq 40 \text{ m}$) were less dense on the eastern side (at 80 Km) than on the western side of the dome. The contrary was true at depths below 60 m where less dense water was on the western side

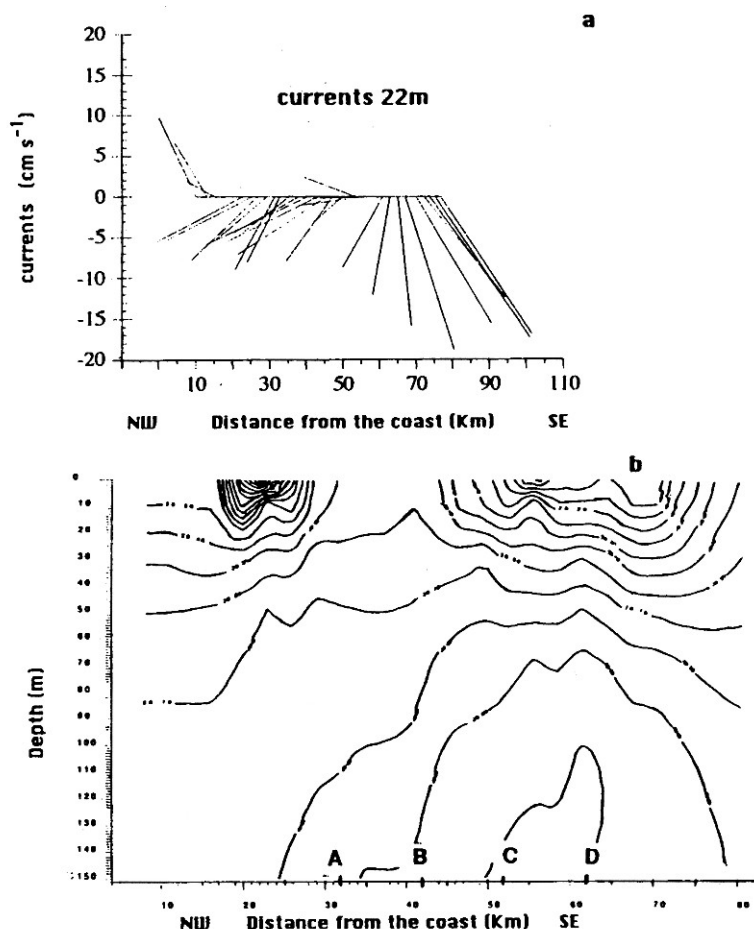


Figure 4. a. ADCP currents measured at a depth of 22 m along transect T5 during the FROTS 91 experiment. b. The vertical distribution of isopycnals across transect T5. Sections A (35 Km), B(42 Km), C(52 Km) and D(62 Km) denote transitions in water masses across the frontal system.

of the dome as a result of the steep downward sloping isopycnals from 10-35 Km (Figure 4b).

Both shear and HKE (Figure 5a) showed marked variation across transect T5, particularly near the convergence zone of the two water masses at 32, 42, 52, and 62 Km (see Figure 4b). Averaged heights between isopycnals for all stations along sections A(32 Km), B(42 Km), C(52 Km), and D(62 Km) (i.e. parallel to the coast) were statistically different ($p=0.0001$) indicating changes in water masses across the front. Along transect T5, the vorticity index, $\frac{h}{h_0}$, was highest in the vicinity of the front (35-55 Km) and corresponded to cyclonic vorticity (Figure 5b). The vorticity index also showed a similar (though not identical) spatial trend as the 22 m potential vorticity (Figure 5b).

4. Discussion

The existence of high energy eddies in the Sargasso Sea, evident in the plots of SSH anomalies, currents, HKE, temperature, and vertical shear, is also evident in the time series of the vorticity indices. The location and rotation of cyclonic and anticyclonic eddies, confirmed by maps of sea surface height,

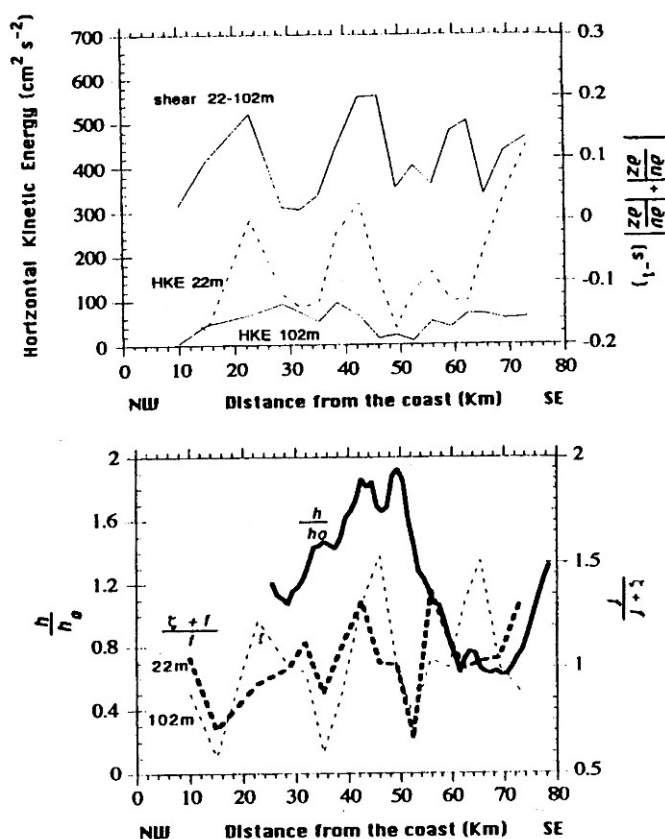


Figure 5. Distributions of flow properties normal to the coast along transect T5. a. HKE at depths of 22 and 102 m and the absolute value of vertical current shear, $\left| \frac{\partial u}{\partial z} + \frac{\partial v}{\partial x} \right|$, between depths of 22 and 102 m. b. Potential vorticity, and the index of vorticity, $\frac{h}{h_0} \frac{f}{f_0}$. The index was calculated based on the difference between the 28.8 and 28.7 kg m⁻³ isopycnals.

qualitatively agree with changes in vorticity indices. Using a mean eddy radius of 50 Km, measured directly from the SSH images, and a maximum velocity of 80 cm s⁻¹ (from both mooring data and geostrophic calculations, Chia et al., 1992), and assuming zero velocity in the center of these eddies, we estimate a relative vorticity of a typical eddy field to be 2×10^{-5} s⁻¹, or $0.25f$. This calculation depends on the energetics of the eddy field which changes over the seasonal scale (Dickey, et., 1993). Nevertheless, similar estimates of relative vorticity ($3.7\text{--}5.0 \times 10^{-5}$ s⁻¹) have been calculated by Olson (1980) for a cyclonic eddy in the Sargasso sea.

The Rossby number, $R_o = \frac{u}{L_f}$, is useful for estimating the contribution of forces in gradient flows, where u is the velocity of the advective system and L is the scale of motion. For large scale eddies, Rossby numbers are low, thus forces associated with planetary vorticity were more important than vorticity resulting from advective effects. However, local time and space scales sampled at the mooring were less than those of large scale eddy fields and therefore provided higher resolution of vorticity changes. On these smaller space and time scales,

the indices of relative vorticity show much larger changes, 2-3 times (Figure 3d). Time series of SSH images also show systems of cyclonic- anticyclonic eddies (note the SSH anomalies with similar dates in Figure 1b) associated with large changes in horizontal current shear and, possibly, frontal jets in the vicinity of the mooring (Chai et al., 1992). Kastanos and Ferentinos (1991) have noted similar changes in vorticity associated with meandering eddies. Woods (1988) has hypothesized such asymmetries in eddy flow fields are coincident with frontal jets. In these current jets, we would expect an increase in the local Rossby number near 1 (Olson, 1980). For the high energy periods of the HKE time series,

L_{jet} can be estimated as $u\tau$ or the time scales between vorticity reversal, $\tau = 3$ days (which is the mean time of PU and PD events), times u , the translational velocity of the eddy system, typically $4-5 \text{ Km d}^{-1}$ (SSH measurements and Richardson, 1983); thus spatial scales are from 12-15 Km. The result, for these high energy periods when measured velocities ranged from $20-80 \text{ cm s}^{-1}$, $0.2 \leq R_o \leq 0.8$ indicating enhanced advective effects possibly associated with current jets.

Along the Catalan front, current measurements reflect a positive (cyclonic), though low, vorticity confirming previous hypotheses of circulation in the region (Font et al., 1988). Maximum relative vorticities along transect 5 (measured from ADCP data) were located between 45 and 55 Km, the same area where $\frac{h}{h_o}$ was maximum, and varied from $0.3f$, at a depth of 22 m, to $0.5f$, at a depth of 102 m. A second relative vorticity maximum, at 102 m, was between 60 and 70 Km. Data of Castellon et al. (1990) confirms the abrupt change in direction and magnitude of currents over a distance of 10 to 20 Km.

The location of the frontal feature is clearly evident in the distributions of HKE, shear, and the vorticity index, $\frac{h}{h_o}$ (Figure 5). All three parameters are highest on periphery of the convergence zone. The vorticity index shows the same tendency for cyclonic circulation associated with the frontal system, however, relative magnitudes are larger than expected, possibly a result of the ambiguity in defining true reference heights, h_o , associated with the meandering fronts. Generally, potential vorticity increased with increasing distance from the Iberian Peninsula. This is consistent conservation of vorticity as the Catalan current shallows along the coast, on the western side of the convergence zone, and the Balearic current deepens on the eastern side of the convergence zone.

5. Conclusions

The simple relationship between isotherm/isopycnal height and relative vorticity seemed to be valid for detection of mesoscale features for both time series and synoptically sampled hydrographic grids. Moored data were collected at one location, with coarse vertical resolution, but high temporal resolution. For these open ocean data, where density was more dependent on temperature than salinity, two indices of vorticity, the number of isotherms below the mixed layer and the distance between two isothermal surfaces, accurately represent the vorticity field, at least quantitatively. The sensitivity of the vorticity indices for the time series (moored data) was dependent on: 1) the strength of the temperature gradient, since fewer isotherms gave less accurate detection; 2) the vertical resolution of the temperature gradients, since fewer samples reduced the accuracy in interpolated isotherms and thus h ; and 3) the time dependent changes in

the gradient - for example, seasonal changes effected the calculation of h_0 , the Sverdrup height.

For the hydrographic survey between the Catalan and Balearic front, the vorticity index based on isopycnals gave reasonable results. The sensitivity of the vorticity index for the hydrographic grid was dependent upon: 1) the vertical and horizontal resolution of density (salinity and temperature) for each water mass present; 2) the synopticity of the survey or how rapidly the mesoscale grid was sampled; and 3) the ability to determine h_0 (parallel to the flow field) for a given water mass.

Complimentary data, such as remotely sensed satellite data (for Sargasso Sea time series) and in situ current data (for the Catalan Sea synoptic survey), were essential in accessing the accuracy of the vorticity indices and in determining the general properties of the flow field.

Acknowledgements

The authors would like to thank all those involved with collection and processing of the Biowatt and Fronts 91 data. Particular thanks to Z. Chai and J. Vazquez (for satellite data) and the crew of the B/O Garcia del Cid. Financial support for field work was provided by CICYT Grant MAR91-0359 to M. Alcaraz. T. Granata was supported by a grant from Ministerio de Educacion y Ciencias (Spain).

References

- Briscoe, M.G., and R.A. Weller. 1984. Preliminary results from the Long-Term Upper-Ocean Study (LOTUS). *Dyn. Atmos. Oceans*, **8**, 243-265.
- Castellón, A., J. Font, and E. Garcia. 1990. The Liguro-Provençal-Catalan current (NW Mediterranean) observed by Doppler profiling in the Balearic Sea. *Sci. Mar.*, **54**(3), 269-276.
- Chai, Z., T. Dickey, J. Vázquez, and J. Wiggert. 1992. Observations of mesoscale features in the Sargasso Sea in 1987 using satellite, ship-based, and mooring measurements. Tech. Report., OPG-91-01, 160pp. University of Southern California, Los Angeles, Calif.
- Dickey, T., E. Hartwig, and J. Marra. 1986. The Biowatt bio-optical and physical moored measurement program. *EOS*, **67**, 650.
- Dickey, T., J. Marra, T. Granata, C. Langdon, M. Hamilton, J. Wiggert, D. Siegel, and A. Bratkovich. 1991. Concurrent high resolution bio-optical and physical time series observations in the Sargasso Sea during the spring of 1987. *J. Geophys. Res.*, **96**, 8643-8663.
- Dickey T., T. Granata, J. Marra, C. Langdon, J. Wiggert, Z. Chai-Jochner, M. Hamilton, J. Vasquez, M. Stramska, R. Bidigare, and D. Siegel. 1993. Seasonal variability of bio-optical and physical properties in the Sargasso Sea. *J. Geophys. Res.*, **98**, 865-898.
- Estrada, M. and R. Margalef. 1988. Supply of nutrients to the Mediterranean photic zone along a persistent front. *Oceanol. Acta, special issue*, **9**, 133-142.
- Fischer, J., H. Leach, and J.D. Woods. 1989. A synoptic map of isopycnal potential vorticity in the seasonal thermocline. *J. Phys. Oceanogr.*, **19**, 519-531.
- Font, J., J. Salat, and J. Tintoré. 1988. Permanent features of circulation in the Catalan Sea. *Oceanol. Acta, special issue*, **9**, 51-57.
- Gill, A.E. 1982. *Atmosphere-Ocean Dynamics. Intl. Geophys. Series*, **30**, 216-217, Academic Press, NY
- Hau, B.L., J.C. McWilliams, and W.B. Owens. 1986. An objective analysis of the POLY-MODE local dynamics experiment. Part II: Streamfunction and potential vorticity fields during the intensive period. *J. Phys. Oceanogr.*, **16**, 506-522.

Joyce, T.M., D. Bitterman, Jr., and K. Prada. 1982. Shipboard acoustic profiling of upper ocean currents. *Deep-Sea Res.*, **29**(7), 903-913.

Kastanos, N. and G. Ferentinos. 1991. Mesoscale current variability in the Otranto Straits, Adriatic Sea. *J. Geophys. Res.*, **96**, 8741-8754.

MODE Group, The. 1978. The Mid-Ocean Dynamics Experiment. *Deep-Sea Res.*, **25**, 859-910.

Olson, D.B. 1980. The physical oceanography of two rings observed by the Cyclonic Ring Experiment. Part II: Dynamics. *J. Phys. Oceanogr.*, **10**, 514-528.

Reigier, L. 1982. Mesoscale current fields observed with a shipboard profiling acoustic current meter. *J. Phys. Oceanogr.*, **12**, 880-886.

Richardson, P.L. 1983. Gulf Stream Rings. In: *Eddies in Marine Science*, 19-45, A.R. Robinson, Ed., Springer-Verlag, Berlin.

Salat, J. and J. Font. 1987. Water mass structure near and offshore the Catalan coast during the winters of 1982 and 1983. *Annales Geophysicae*, **5B**(1), 49-54.

Strass, V. and J.D. Woods. 1988. Horizontal and seasonal variation of density and chlorophyll profiles between the Azores and Greenland. In: *Toward a Theory on Biological-Physical Interactions in the World Ocean*, 113-136, B.J. Rothschild, Ed., Kluwer Academic Publishers.

Washburn, L., B.H. Jones, A. Bratkovich, T. Dickey, and M-S Chen. 1993. Mixing, dispersion and resuspension in the vicinity of an ocean wastewater plume. *J. Hydraul. Engin.*, in press.

Weller, R., and R.E. Davis. 1980. A vector measuring current meter. *Deep-Sea Res.*, **27**, 565-582.

Woods, J.D. 1988. Scale upwelling and primary production. In: *Toward a Theory on Biological-Physical Interactions in the World Ocean*, 7-38, B.J. Rothschild, Ed., Kluwer Academic Publishers.